Satellite Debris: Recent Measurements

L. G. Taff*
Massachusetts Institute of Technology, Lincoln Laboratory, Lexington, Massachusetts

Increasing reports of hazards to spacecraft owing to debris, the replacement of a window on one of the space shuttles (STS-7) following an impact, and recent observational work on the debris population prompt this paper. The Space Surveillance group of M.I.T.'s Lincoln Laboratory has been engaged in the creation, design, development, and testing of equipment and techniques to observe moving objects by passive optical means for over a decade. With regard to artificial satellites, asteroids, and meteors, we have created the state-of-the-art observing systems for both the U.S. Air Force and NASA. One of the by-products of our research efforts has been the measurement of the untracked artificial satellite population in both the near-Earth and the deep-space realms. This paper consolidates hundreds of hours of observation on space debris, briefly describes our observing techniques, quantifies the numbers of small bodies in space relative to the actively watched artificial-satellite population, and estimates the numbers of detectable objects from 1 cm (near-Earth) to 20 cm (near-stationary distances). There is a lot of debris in orbit—at least 11 times the tracked population of satellites in near-Earth orbit and at least 25%, and probably 50%, of the deep-space population. Moreover, the deep-space debris is situated in all the common deep-space orbits.

Nomenclature

a = semimajor axis of a satellite's orbit
B = apparent blue magnitude on the Johnson UBV system
B_S = B for the sun = $-26^m.1$
D = linear size of piece of debris
e = eccentricity of a satellite's orbit
GM_E = Newton's universal constant of gravitation times the mass of the Earth
i = inclination of a satellite's orbit
n = mean motion of a satellite's orbit; related to a by Kepler's third law, $n^2a^3 = GM_E$
$p\phi$ = product of geometric albedo and phase law for a satellite
r,R = heliocentric and topocentric distances of a satellite, respectively
s = slope of satellite streak on telescope's focal plane
μ = angular speed on telescope's focal plane
τ = local mean sidereal time
ϕ' = geocentric latitude of observer
Ω = longitude of ascending node of a satellite's orbit

Introduction

As man's activities in space have matured, become more frequent, and encompassed more varied purposes, the remnants of these activities have proliferated and spread. This is most notable in cislunar space, especially in the very near-Earth environment. Orbital inclinations at some elevations are so crowded with artificial "meteoroids" that they are already hazardous to manned spacecraft. In this paper I report on state-of-the-art optical measurements of the uncataloged artificial-satellite debris population in both the near-Earth (elevations $\leq$ 1500 km) and the "deep-space" realms. The results may be briefly summarized as follows: Relative to the North American Defense Command (NORAD) catalog of artificial satellites, near-Earth debris is 11 times as populous as are known objects. Deep-space debris is present in numbers equal to at least one-quarter of the tracked population. These two results refer to different limiting magnitudes ($B = 16^m.5$ and $17^m.7$) and to two different sizes; 1 cm for the near-Earth objects, 20 cm for those at geosynchronous distances. Following is a brief description of the observatory where the work was performed and an outline of the different techniques used to discover and track debris.

The Observatory

The observatory is known as the Lincoln Laboratory Experimental Test System (ETS). It was designed and built for the development and evaluation of optical space surveillance techniques for the U.S. Air Force's GEODSS (Ground-based Electro-Optical Deep Space Surveillance) network. This duplex facility is located about 50 km southeast of Socorro, New Mexico (geodetic latitude = + 33 deg 49 min). Each dome contains two comounted polar-axle telescopes (see Fig. 1). The larger is an 80-cm, $f/5$ Ritchey-Chretien instrument with a nominal $1^\circ.2$ field of view at the Cassegrain focus across a flat 80-mm focal plane. In the prime focus configuration, it is $f/2.87$ with a 2-deg field of view. The smaller instrument is a 36-cm, $f/1.7$ folded Schmidt with a 7-deg field of view (see Fig. 2). Both the domes and the instruments within are under interactive computer control. Each set is remotely operated from its own console (see Fig. 3). The separation between the telescope mounts is 59.23 m.

The cameras attached to the telescopes use state-of-the-art, low-light-level, beam-scanned television camera tubes of the intensified silicon diode array type, generally known as EBSICONs. They can be characterized as having high sensitivity (180 μA/1m), adequate image cell size ($\simeq$ 4 arc sec with our plate scale), moderate charge storage capability (10^6 per image cell), high prescanning gain ($>$ 2000), good dynamic range (300 at fixed potential), acceptable saturation characteristics (1 μA), and an almost burnproof target. Moreover, they can be packaged in a rugged, simple-to-operate fashion. Their overall performance may be characterized as being photon-noise limited under dark skies. The basic frame repetition interval is 1/30 sec. Finally, a single-stage image intensifier in front of the EBSICON device can provide additional gain and a 2:1 demagnification.

Most functions are performed by using preprogrammed buttons at the operating console (see Fig. 3). The MODCOMP IV-25 computer with extended storage, large and fast disk drives, and a variety of attached microprocessors shuffles several software packages asynchronously via the master real-time operating system. The two largest files to which it has fast access are the NORAD deep-space catalog of $\simeq$ 600 orbital

Received May 6, 1985; revision received Oct. 7, 1985.

*Member Technical Staff, Aerospace Division, Space Surveillance Group.

element sets and the Smithsonian Astrophysical Observatory Star Catalog.[1] The astrometric and photometric functions performed are akin to those used in minor planet work, appropriately modified for the real-time environment. More detailed overviews of the observatory and the camera systems have been published.[2,3]

Following a successful proof-of-concept demonstration, the U.S. Air Force proceeded to procure a five-site operational GEODSS network[4] as a replacement for the Baker-Nunn camera system. The ETS then became more available for other types of observing programs. It has been modified to search for Earth-approaching asteroids at state-of-the-art rates and sensitivities[5,6] and to observe near-Earth satellites in full daylight.[7] Other unusual uses of the observatory include the monitoring of satellite launches. While the deep-space searches outlined below are a fundamental reason for the GEODSS network, the near-Earth searches required a significant reconfiguration of the video processing system at the observatory.

Deep-Space Debris Search

The "deep-space" population of artificial satellites can be partitioned into three classes. One class is the near-stationary satellites. These satellites have low inclinations ($i \leq 20$ deg), small eccentricities ($e \leq 0.2$), and mean motions near one revolution/day ($0.9 \leq n \leq 1.1$ rev/day). This is the second most populous class of known satellites (representing about 30%). The most populous class of deep-space satellites can be characterized by shorter periods (generally $n > 2$ rev/day). Usually they have higher inclinations [with large numbers of satellites near $i \simeq 30$ deg (16%) and $i \simeq 62$ deg (40%)] and larger eccentricities. The third class contains the remainder.

Deep-space artificial-satellite apparent angular speeds vary over the range 6-300 arc sec/sec. Their characteristic dimensions cover the interval from 1-30 m. A few typical examples are shown in Fig. 4. Active payloads are generally stabilized with respect to a spin axis or the sun, while inactive payloads, rocket bodies, and pieces of debris generally tumble freely in orbit.

Two telescope searches were performed ($\simeq 150$ square deg/h) wherein one telescope actually did the searching and preliminary object discrimination and the other telescope performed all the other functions, such as the final discrimination decision on the newly discovered satellite, specialized small-area searches, astrometric data acquisition, and photometric data acquisition. The near-stationary search strategy used is to sweep the topocentric equator at a rate of one hour of right ascension per hour of time. The extent in declination is constrained by the field of view of the telescope, the rapidity with which the telescope can be moved and stopped, the time

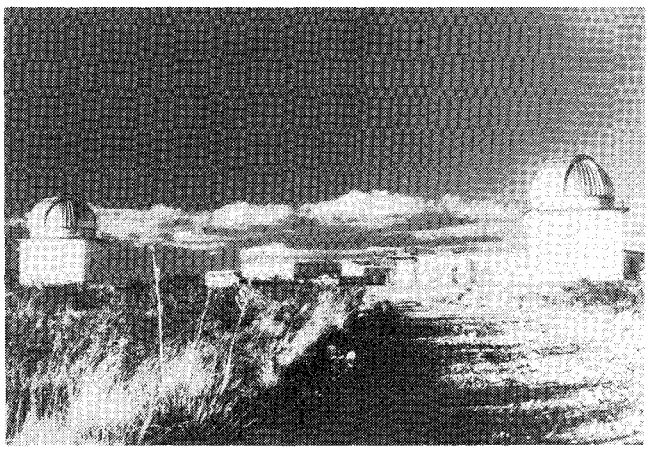

Fig. 1 The Lincoln Laboratory Experimental Test System viewed from the west.

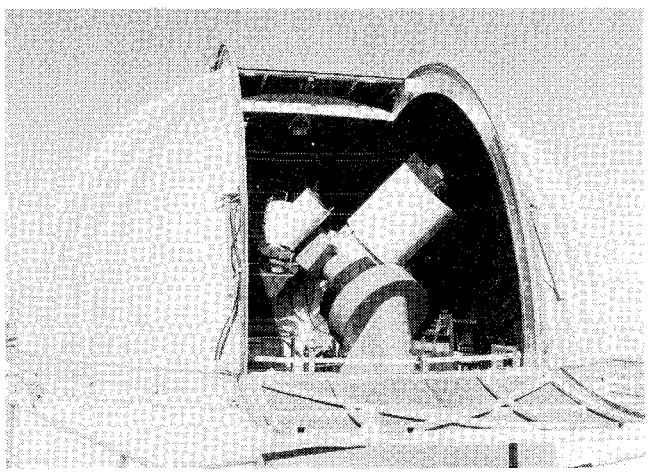

Fig.2 The ETS telescope showing the wide dome slits and the wind screen down.

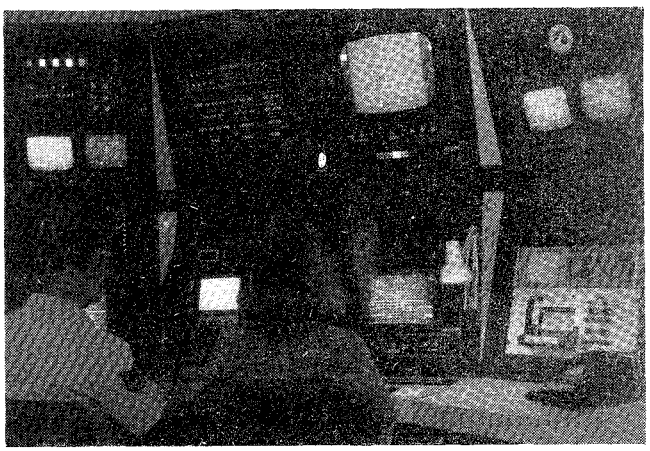

Fig. 3 View of one of the telescope operating consoles.

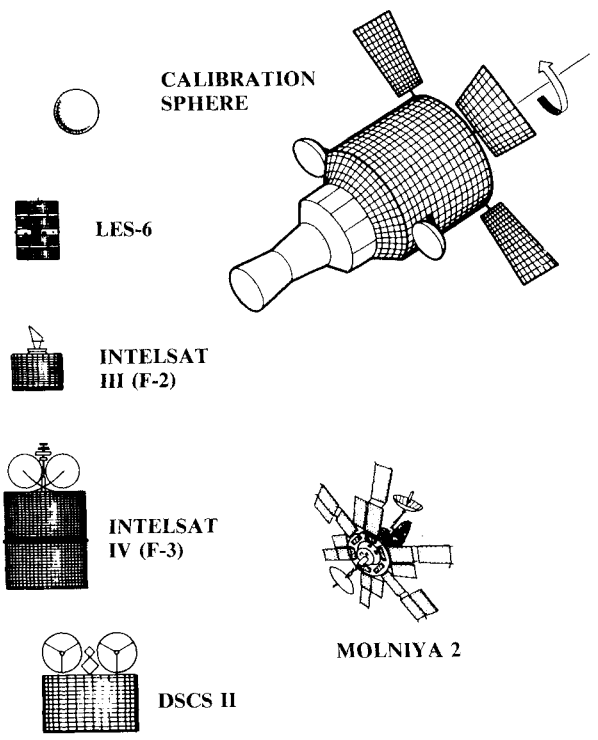

Fig. 4 A few typical satellite shapes (not to scale).

needed to handle detections, and so forth. The declination extent is $\simeq 12$ deg. Searches for high-inclination satellites were performed by scanning a fence along the celestial meridian.

Approximately one piece of debris was found per hour of search in both the near-stationary and high-inclination searches. Because these searches were carried out over the course of several "specular seasons" in the late 1970s, the data base is hundreds of hours long. The orbital element sets of the objects detected are typical of the tracked population and will not be reproduced here. The presence of deep-space debris is widespread in all the common deep-space orbits. Indeed, in one instance, we found four untracked satellites in a single 1°.2 field of view.

The brightness variations of these objects rarely showed the stabilized rotation characteristic of actively maintained payloads. Figure 5 shows a typical payload light curve.

Because the principal purpose of these efforts was to test observing procedures, search strategy, and celestial mechanics tools,[8,9] precise records were not always kept of the cataloged-to-known ratio. Abstracting from our notes and collective memory, I can be sure that debris represents at least one-quarter of the tracked population in deep space[10] and possibly as much as one-half of it at this limiting magnitude ($B = 17^m.7$). From photometry one can approximate the luminosity function in this magnitude range; it is a positively increasing exponential function.

Near-Earth Debris Search

The methods and analysis necessary for the near-Earth searches are totally different from the near-stationary or high-inclination searches. The reason is the probability of contamination by meteors, which a single telescope cannot discriminate against. Only by having two nearly identical instruments, equipped with nearly identical equipment, can one use parallax to eliminate meteors confidently. Also, because of the speed with which these objects move, photometric calibrations were especially difficult to carry out.

The most difficult engineering aspect of this work was the maintenance of an optimum alignment between the two EBSICON cameras. The video intensity levels, the synchronization and blanking levels, and both the horizontal and vertical sweep voltages (which fix the effective field sizes) had to be fine-tuned throughout the observing period. In addition, the direction of the electron beam sweep had to be kept parallel to the parallels of declination to avoid field rotation.

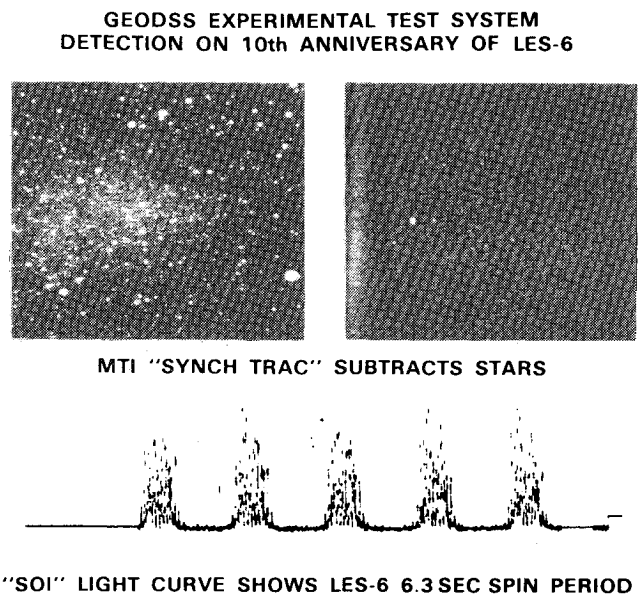

Fig. 5 A typical light curve. The satellite is Lincoln Experimental Satellite No. 6.

The best we were able to do was to keep the inner two-thirds of the fields of view aligned to within a video scan line. Having aligned the telescopes and cameras, we then attached the videotape recorders, the time synchronization equipment, and so on. As in very long baseline (VLBI) work, the key to an accurate reconstruction of the video signals is the synchronization of a shared time code. We used SMPTE (Society for Motion Picture and Television Engineers) time code to perform frame-to-frame matching. Because each videotape contains impressions of the stars, various artificial satellite tracks, and meteor passes, it is necessary to discriminate among them. While angular speed can serve as a discriminator between most near-Earth satellites and meteors, the use of parallax and angular speed provides an almost perfect means of separating the two phenomena. In order to facilitate the detection of a parallax, it is desirable to have the two video sequences overlaid. In addition, the removal of the stellar background would aid in the examination of the videotapes. Finally, some suppression of the noise in the cameras (which typically shows as scintillations) and a general smoothing of the night sky background are desirable, too.

Our 50% probability of detection magnitude on the processed videotapes is $B = 16^m.5$ when objects are moving $\simeq 0°.5$/sec. This degraded by about 2^m per 1 deg/sec near 0°.5/sec and refers to good atmospheric conditions (e.g., extinction per unit air mass $< 0^m.25$).

To compute the size of the pieces of debris, I used the usual planetary photometry formula

$$\log(rR/D) = 0.5 \log(p\phi) + (B - B_S)/5 \qquad (1)$$

Taking $r = 1$ a.u., $D = 1$ cm, and for $p\phi$ an optimistic value of unity, implies that $R = 3300$ km for $B = 16^m.5$. For darker objects seen near quadrature (the phase angle for most of these objects is $\simeq 90$ deg), say $p\phi = 0.1$, the corresponding value of R is 1050 km.

In the search for near-Earth artificial satellites and their debris, the satellites must be illuminated by the sun while the

Table 1 Hourly rates of meteors and satellites

	Meteors		Satellites	
	Raw[a]	Corrected	Raw	Corrected
Evening	1.5	5.0	4.3	14.5
Morning	6.5	6.5	14.5	14.5
Ratio	4.4	1.3	3.4	1.0

[a]Raw rates are corrected for incompleteness; corrected rates are also adjusted for weather-related factors.

Table 2 Satellite elevation distribution[a]

Bin, km	Corrected for weather	Also corrected for visibility	Normalized to 10^3 km
<300	39.5	245	1250
300-400	4.0	20.3	58.1
400-500	0	0	0
500-600	6.9	10.7	19.5
600-800	3.4	4.1	5.9
800-1000	13.7	13.7	15.2
1000-1200	12.3	12.3	11.2
1200-1400	2.0	2.0	1.5
1400-1600	10.9	10.9	7.3
1600-2000	9.9	9.9	5.5
2000-2500	0	0	0
2500-3000	0	0	0
3000-4000	9.9	9.9	2.8
>4000	14.3	14.3	

[a]Based on 9.3 h of observation.

observatory is in darkness. It is geometrically clear that the only times of day when the circumstances can be favorable are the dusk and dawn twilight hours. (The primary elevation range of interest was 500-1100 km; the secondary ranges were 300-500 and 1100-2000 km.)

There are two other aspects to mention. As of this writing, we could not, because of external time constraints, perform observations in any season other than winter. Therefore, there is the possibility that the lower end of the elevation range was poorly probed. It would be interesting to repeat this experiment near the summer solstice. The other point concerns evening vs morning twilight. From the appearances of the tape recordings, it is evident that visibility and other qualities of the atmosphere are much better during dawn than during dusk. The result is a loss of 1-2^m of sensitivity from dawn twilight to dusk twilight.

Over seven evenings and two mornings in late January and early February of 1984, with no interference from the moon, we accumulated hour-long simultaneous videotape recordings. The videotapes were then viewed and the sightings checked against a similar record made in real time by a different team member. Finally, a third individual reviewed somewhat more than half of all the processed tapes. By comparing the three independent records and by viewing selected samples of the unprocessed videotapes, I could confidently calculate an incompleteness factor. Sufficient morning and evening tapes were examined to deduce their separate incompleteness factors as well. Using these factors, I computed the rates of satellite sightings (see Table 1).

Such rates need to be corrected for three additional sources of systematic error. One is a reduced limiting magnitude during the evening owing to poor atmospheric conditions. The second source of systematic bias is due to the rapidly changing nature of the solar illumination. During dusk the shadow cone of the Earth rises so that at the commencement of evening twilight all elevations are well lit, but near the end only the highest elevations are still in sunlight. The reverse takes place during the development of dawn. Therefore, one cannot discover a very close satellite near the end of evening twilight (because it is eclipsed) while one can find such an object only near the end of morning twilight. The final correction accounted for the nature of the volume of space probed by the search. Clearly this is a cone and, therefore, the slant area varies with elevation.

From the time of occurrence and the time development of each streak, one can deduce the geocentric distance from the measured angular speed (assuming a nearly circular orbit), the inclination of the orbital plane, the longitude of the ascending node, and the elevation from the measured parallax (see below). Ideally, all the orbital and geometrical calculations would follow from a detailed analysis of the appearance of the nearly zenithal pass of a nearly circular, near-Earth artificial satellite. The lowest-order approximation suffices in practice; the result is

$$\mu = na/(a-R_E), \qquad n^2a^3 = GM_E \tag{2}$$

$$\cos i = \pm \cos\phi'/(1+s^2)^{1/2}$$

$$\Omega = \tau - \tan^{-1}[\sin\phi' \cos i/(\sin^2 i - \sin^2\phi')^{1/2}] \tag{3}$$

The plus or minus sign ambiguity can be visually resolved; the plus sign is for direct orbits. The measurement error (of the actual streak on the processed videotapes) is the dominant source of error.

A visual impression might help the reader. A typical bright satellite streak exhibiting parallax is shown in Fig. 6. Figure 7 illustrates a rare double meteor. The parallax is very large compared to that in Fig. 6.

As meteors are a by-product of this research, I have not attempted a sophisticated analysis of the meteors observed. I do believe, however, that these observations represent the largest

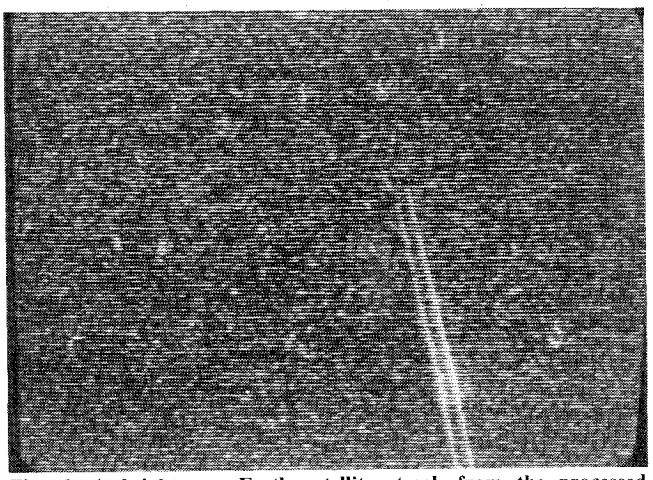

Fig. 6 A bright near-Earth satellite streak from the processed videotapes, showing parallax.

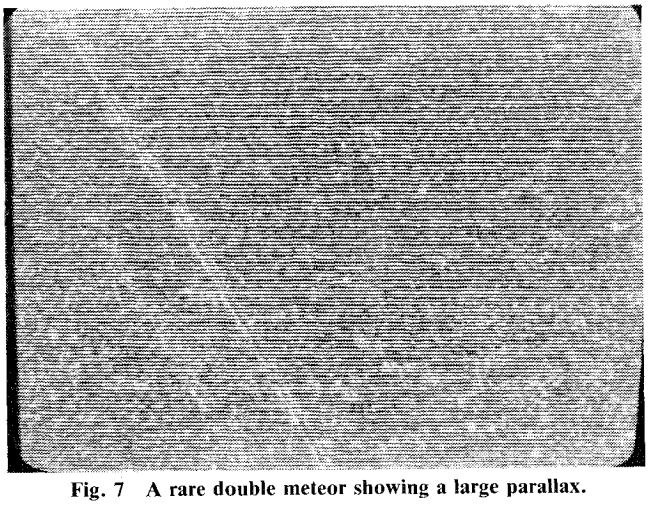

Fig. 7 A rare double meteor showing a large parallax.

stretch of bi-telescopic meteor observations ever performed. Aside from some double meteors (see Fig. 7), which were visually very interesting, the most important result concerns the hourly rates. The raw morning/evening ratio is within the 3-5 range usually quoted. However, the satellite morning/evening ratio is only 2.7. I am certain that the satellite morning/evening ratio departure from unity is because of the 1-2^m loss of sensitivity during evening twilight. This correction is included in the second columns of Table 1 and puts the morning/evening meteor ratio at a low value of 1.3.

The satellite elevation distribution is given in Table 2 at three different stages of adjustment. The first column gives the results after correction for incompleteness and the evening/morning sensitivity loss. The second column includes corrections for the height of the Earth's shadow cone. Finally, normalizing all the elevations to a common cross section (at 1000 km) yields the third column of Table 2. I have provided each of the intermediary distributions so that other workers may smooth or adjust the values according to their own taste.

The hourly rates in Table 1 are a factor of 11 times higher than that predicted from the satellite population currently cataloged by NORAD. This fact, and any reasonable smoothing of the < 300-km bin, implies a much larger debris population than was previously believed to be the case.

The conclusion stated above represents my best estimate of the near-Earth debris population from these data and the described analysis. There are three qualifications to be made. First, this estimate is based on 9.3 h of observation. Moreover, most of it was performed during the poorer evening twilight period. Hence, there is the possibility of a biased sample. Only

many more hours of observation can clarify this point. (Such observations are already under way.) A statistically unshakable sample will be collected by July 1986. Second, the mathematical analysis in Eqs. (2) and (3), and the formulas used for the parallax-based height deduction, are the lowest-order result. A more refined analysis of the celestial mechanics and viewing geometry should be performed and then these observations re-reduced. This too is under way. All the new observations will be reduced, utilizing the results of the more sophisticated treatment, too. Finally, there is an unexplored possibility of systematic measurement errors for the faintest streaks. The cause is simple: the eye/brain combination is extraordinarily adept at picking out moving objects even when the signal-to-noise ratio is near unity. Once the advantage of motion is lost, as it is when the stop frame mode of the videotape recorders is used, the fainter streaks merge with the background. This can also occur because of variations between the sensitivities of the cameras. When the much more extensive sample of observations is treated with refined astrometric and (as yet uninvented) photometric reduction procedures, then the debris population estimates will be definitive.

Summary

This paper summarizes deep optical measurements on near-Earth and deep-space orbital debris. Using the NORAD catalog as representative of the known artificial-satellite population, near-Earth debris is pervasive, 11 times the NORAD density. This type of object down was observed to 1 cm in size. In the 12-24-h orbital period realm, there is also a considerable population of untracked objects, at least 25% and possibly 50% of the NORAD catalog. Barring specular reflections, these objects were seen down to 20 cm. Clearly, in both cases, there are large numbers of objects beyond the capabilities of the current space-tracking sensors.

Acknowledgments

This work was sponsored by NASA and the Dept. of the Air Force under ESD contract F19628-85-C-0002. The near-Earth observations described herein were performed with the assistance of D. E. Beatty, A. J. Yakutis, and P. M. S. Randall and were sponsored by NASA (Johnson Space Center). The deep-space work was sponsored by the U. S. Air Force and conducted with D. E. Beatty, R. L. Irelan, I. M. Poirier, N. G. S. Pong, E. W. Rork, J. M. Sorvari, L. Ward, and A. J. Yakutis.

References

[1]Staff of the Smithsonian Astrophysical Observatory, "Star Catalog," Smithsonian Institution Publication No. 4652, Washington, DC.

[2]Weber, R., "Large-format Ebsicon for Low-Light-Level Satellite Surveillance," *SPIE,* Vol. 203, Aug. 1979, pp. 6-11.

[3]Weber, R., "Passive Ground-Based Electro-Optical Detection of Artificial Earth Satellites," *Optical Engineering,* Vol. 18, Jan.-Feb. 1979, pp. 82-91.

[4]Beatty, J. K., "The GEODSS Difference," *Sky and Telescope,* Vol. 63, May 1982, pp. 469-473.

[5]Taff, L. G., "A New Asteroid Observation and Search Technique," *Publication of the Astronomical Society of the Pacific,* Vol. 93, Oct. 1981, pp. 658-660.

[6]Taff, L. G., "Optimal Searches for Asteroids," *Icarus,* Vol. 57, Feb. 1984, pp. 259-266.

[7]Rork, E. W., Bergemann, R. J., Lin, S. S., Sorvari, J. M., and Yakutis, A. J., "Ground-Based Electro-Optical Surveillance of Satellites in Daylight by Detection of Reflected Sunlight, "*Proceedings of IEEE EASCON '83,* 1983, pp. 103-110.

[8]Taff, L. G. and Sorvari, J. M., "Differential Correction for Near-Stationary Satellites," *Celestial Mechanics,* Vol. 26, April 1982, pp. 423-431.

[9]Taff, L. G. and Hall, D. L., "The Use of Angles and Angular Rates," *Celestial Mechanics,* Vol. 16, Dec. 1977, pp. 481-488.

[10]Rork, E. W. and Yakutis, A. J., "Searches for Artificial Satellites Conducted with the GEODSS Experimental Test System in the Equatorial Geosynchronous Belt during the Spring, 1978 Specular Season," *Proceedings of the Tenth NORAD Spacecraft Identification Conference,* 1978, pp. 292-345.